

# On X-ray Optical Depth in the Coronae of Active Stars

Paola Testa<sup>1</sup>, Jeremy J. Drake<sup>2</sup>, Giovanni Peres<sup>3</sup>, David P. Huenemoerder<sup>1</sup>

## ABSTRACT

We have investigated the optical thickness of the coronal plasma through the analysis of high-resolution X-ray spectra of a large sample of active stars observed with the High Energy Transmission Grating Spectrometer on *Chandra*. In particular, we probed for the presence of significant resonant scattering in the strong Lyman series lines arising from hydrogen-like oxygen and neon ions. The active RS CVn-type binaries II Peg and IM Peg and the single M dwarf EV Lac show significant optical depth. For these active coronae, the  $\text{Ly}\alpha/\text{Ly}\beta$  ratios are significantly depleted as compared with theoretical predictions and with the same ratios observed in similar active stars. Interpreting these decrements in terms of resonance scattering of line photons out of the line-of-sight, we are able to derive an estimate for the typical size of coronal structures, and from these we also derive estimates of coronal filling factors. For all three sources we find that the both the photon path length as a fraction of the stellar radius, and the implied surface filling factors are very small and amount to a few percent at most. The measured  $\text{Ly}\alpha/\text{Ly}\beta$  ratios are in good agreement with APED theoretical predictions, thus indicating negligible optical depth, for the other sources in our sample. We discuss the implications for coronal structuring and heating flux requirements. For the stellar sample as a whole, the data suggest increasing quenching of  $\text{Ly}\alpha$  relative to  $\text{Ly}\beta$  as function of both  $L_X/L_{\text{bol}}$  and the density-sensitive Mg XI forbidden to intercombination line ratio, as might generally be expected.

*Subject headings:* Radiative transfer — X-rays: stars — stars:coronae — stars:late-type

---

<sup>1</sup>Massachusetts Institute of Technology, Kavli Institute for Astrophysics and Space Research, 70 Vassar street, Cambridge, MA 02139, USA; testa@space.mit.edu

<sup>2</sup>Smithsonian Astrophysical Observatory, MS 3, 60 Garden Street, Cambridge, MA 02138, USA

<sup>3</sup>Dipartimento di Scienze Fisiche & Astronomiche, Sezione di Astronomia, Università di Palermo Piazza del Parlamento 1, 90134 Palermo, Italy

## 1. Introduction

A fundamental issue in the physics of stellar outer atmospheres concerns the relationship between magnetic activity on stars with a wide range of physical parameters and solar magnetic activity. How directly and how far does the solar analogy apply to other stars, and do any of the underlying physical processes differ? The X-ray luminosities of late-type stars can span several decades (e.g., Vaiana et al. 1981), and these hot coronae are found on such a wide range of spectral types that the extrapolation of the now well-studied solar corona to the extremes of stellar activity is by no means obvious and could be inappropriate. Indeed, “scaled up Sun” scenarios, in which a stellar surface is covered with bright solar-like active regions, only realise X-ray luminosities 100 times that of the typical active Sun (e.g., Drake et al. 2000). The most active stars, with X-ray luminosities of up to 10,000 times the solar X-ray luminosity, must have coronae which are structured differently in some way.

Since coronal structures can be imaged presently only on the Sun, the structuring of other stellar coronae is generally investigated through the application of techniques such as the study of lightcurves during flares (e.g., Schmitt & Favata 1999; Favata et al. 2000a; Maggio et al. 2000; Reale et al. 2004; Testa et al. 2007), rotational modulation (e.g., Brickhouse et al. 2001; Marino et al. 2003; Huenemoerder et al. 2006), and study of density properties together with information on emission measure (e.g., Testa et al. 2004a, hereafter TDP04; Ness et al. 2004). Most of these analyses indicate that the emitting plasma is rather compact (scale height  $\leq 0.5R_*$ ) and localized at high latitude (see e.g., Schmitt & Favata 1999; Brickhouse et al. 2001; Testa et al. 2004b, TDP04); however, the presence of extended coronal plasma has also been claimed on some stars based on UV and X-ray Doppler studies (e.g. Chung et al. 2004; Redfield et al. 2003).

The search for signs of quenching in strong lines through resonance scattering represents a further technique that offers a potentially powerful diagnostic of the sizes of X-ray emitting regions; the escape probability of a photon emitted by a resonance line in a low density homogeneous plasma is in fact dependent on the line-of-sight path length through the plasma region. Significant scattering optical depth can be combined with density measurements to obtain an estimate of photon path length within the emitting plasma.

Several existing studies have explored optical depths of both solar and stellar coronal emission lines. Studies of solar X-ray spectra have aimed at probing the optical depth in the strong ( $gf = 2.66$ )  $2p^53d^1P_1 - 2p^6^1S_0$  resonance line of Fe XVII at 15.01 Å as compared to nearby weaker Fe XVII lines, though with controversial results concerning whether optical depth effects were seen or not (Phillips et al. 1996, 1997; Schmelz et al. 1997; Saba et al. 1999). In particular, Saba et al. (1999) review recent observational findings on the opacity inferred from the study of the bright iron resonance line at 15.01 Å and on the center-

to-limb behaviour. Among other issues, Saba et al. (1999) address the discrepancy they find in the derived direction and magnitude of the center-to-limb trend (also in agreement with Schmelz et al. 1997), as compared to the findings of Phillips et al. (1996) who find that the effect of resonant scattering is decreasing from the disk center toward the solar limb, a trend irreconcilable and totally opposite to that found by Saba et al. (1999) and Schmelz et al. (1997). Brickhouse & Schmelz (2006) have recently reanalyzed solar X-ray spectra and suggest that previously ignored blends might explain the departure of measured ratios from theoretical calculations.

Resonant scattering in stellar coronae has been investigated by Phillips et al. (2001) and Ness et al. (2003) through the analysis of the same transition observed at high resolution ( $\lambda/\Delta\lambda$  up to  $\sim 1000$ ) by *Chandra* and XMM-*Newton*. Both stellar studies of Fe XVII transitions fail to find evidence for significant deviation from the optically thin regime, and in particular the large survey of stellar spectra analyzed by Ness et al. (2003) show that no firm results can be obtained from Fe lines. One exception is the suggestion of resonance scattering in Fe XVII 15.01 Å on the basis of the observed variability of line ratios seen during a flare on AB Dor by Matranga et al. (2005). We note that Phillips et al. (2001) attempted to derive constraints on emitting region size based on their upper limit to optical depth in the coronae of Capella, though, as we discuss in this paper (§6), such upper limits cannot be reliably used in this fashion because scattering *into* the line of sight renders optical depth measurements themselves only lower limits to the true scattering depth.

In a previous *Letter* (Testa et al. 2004b, hereafter Paper I) we presented results obtained using a different approach to the study of coronal optical depth, through the analysis of Ne and O Ly $\alpha$  to Ly $\beta$  line strength ratios as observed by the High Energy Transmission Grating (HETG) on board the *Chandra* X-ray Observatory. Significant depletion of Ly $\alpha$  lines to resonance scattering were seen in the spectra of the RS CVn-type binaries II Peg and IM Peg. In this paper we follow up on that exploratory study and examine the Ne and O Lyman series lines in a large number of active stars (namely, the same sample for which the plasma density was analysed in TDP04) in order to survey the X-ray optical depth properties of active stellar coronae.

We discuss in §2 the advantages of the Lyman series analysis with respect to the “standard” approach using Fe XVII lines. The observations are briefly described in §3. Our techniques of line flux measurement and spectral analysis are described in §4. The results are presented in §5. We combine the results of this study with our earlier density estimates and discuss these in the context of coronal structure on active stars in §6; we draw our conclusions in §7.

## 2. Resonant scattering in Ne and O Lyman series lines.

The Fe XVII soft X-ray complex at  $\sim 15\text{\AA}$  has been a primary tool to probe coronal optical depth because of the large oscillator strength of the  $2p^6\ ^1S_0-2p^53d^1\ P_1$  15.01  $\text{\AA}$  resonance line and its consequent prominence in solar spectra. However, Doron & Behar (2002) and Gu (2003b) have recently shown that the indirect processes of radiative recombination, dielectronic recombination, and resonance excitation involving the neighbouring charge states are important for understanding the relative strengths of Fe XVII–XX lines. There is thus still some considerable difficulty in reconciling theoretical and observed line strength ratios. Recently, Brickhouse & Schmelz (2006) have found good agreement of solar observed ratios with new theoretical calculations (Chen & Pradhan 2005), and suggest that center-to-limb observed trends (Phillips et al. 1996; Schmelz et al. 1997; Saba et al. 1999) are due to chance rather than to optical depth effects.

An additional problem in using Fe XVII lines as diagnostics of optical depth is that this element has been found to be *depleted* in the coronae of active stars by factors of up to 10 (e.g., Drake et al. 2001; Huenemoerder et al. 2001; Drake 2003; Audard et al. 2003) as compared with a solar or local cosmic composition. The ratio of the line-center optical depths,  $\tau_i/\tau_j$ , of two lines  $i$  and  $j$  is given by

$$\frac{\tau_i}{\tau_j} = \frac{f_i \lambda_i \phi_i A_i \sqrt{m_i}}{f_j \lambda_j \phi_j A_j \sqrt{m_j}} \quad (1)$$

where  $f$  is the oscillator strength,  $\lambda$  is the wavelength,  $\phi$  is the fractional population of the ion in question,  $A$  is the element abundance and  $m$  the ion mass. The line optical depth is directly proportional to abundance and, in the case of stellar coronae, where only the very strongest spectral lines might be expected to undergo any significant resonance scattering, any abundance depletions also reduce the sensitivity of lines as optical depth indicators. For coronal abundances typically found in RS CVn systems (see e.g. reviews by Drake 2003; Audard et al. 2003), we expect resonant lines from the more abundant ions like oxygen and neon to be more sensitive to resonant scattering processes than the resonant Fe XVII line. This is illustrated in Figure 1, where we show the relative optical depths for the O VIII and Ne X Ly $\alpha$  lines and the Fe XVII  $\sim 15.01\ \text{\AA}$  resonance line for both a representative solar chemical composition (Grevesse & Sauval 1998) and for a chemical composition typically found for active stars. For the latter, we assumed Ne and Fe abundances 0.3 dex higher and 0.5 dex lower, respectively, than the corresponding solar values; we note that in several active coronae abundance anomalies even more pronounced have been found (e.g., Brinkman et al. 2001; Huenemoerder et al. 2001).

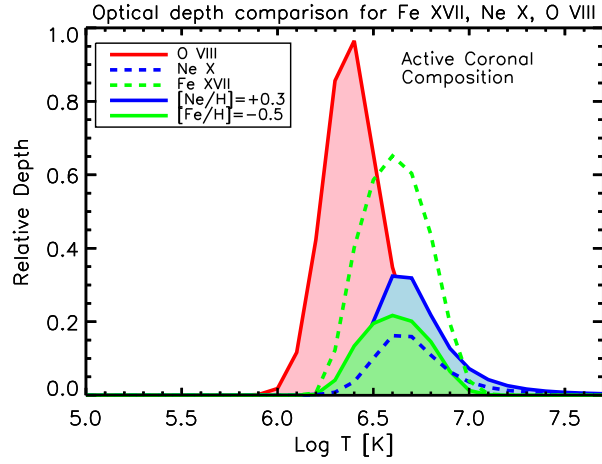


Fig. 1.— The relative sensitivity of Ly $\alpha$  lines of Ne X, O VIII, and the strong Fe XVII 15.01 Å transition to resonant scattering, as a function of plasma temperature. Relative line optical depths, normalised to the maximum depth in O VIII, are shown for two sets of abundances. Dashed lines correspond to the solar photospheric abundance mixture of Grevesse & Sauval (1998); filled profiles correspond to coronal abundances typically found in RS CVn’s (see text). Because of the typically higher Ne abundance and lower Fe abundance found in the coronae of RS CVn systems, the expected resonant scattering effects are greater for O VIII and Ne X Ly $\alpha$  than for the Fe XVII.

As discussed in Paper I, the effect of resonance scattering of Ly $\alpha$  and Ly $\beta$  photons can be diagnosed by comparison of the measured Ly $\alpha$ /Ly $\beta$  ratio with respect to the theoretical ratio. In principle, both  $n = 2 \rightarrow 1$  Ly $\alpha$  and  $n = 3 \rightarrow 1$  Ly $\beta$  lines can be affected by resonant scattering: when a large optical depth is reached in Ly $\alpha$ , an enhanced population of the  $n = 2$  level can lead to a potentially confusing enhancement in Ly $\beta$  (and Ba $\alpha$ ) through collisional excitation of the  $n = 2 \rightarrow 3$  transition. However, in the limit of fairly small scattering optical depth that we expect to characterize stellar coronae, Ly $\beta$  essentially remains optically thin and should make a reliable comparison with which to diagnose optical depth in Ly $\alpha$ .

### 3. Observations

*Chandra* High Energy Transmission Grating Spectrometer (see Canizares et al. 2000, 2005 for a description of the instrumentation) observations of 22 cool stars covering a wide range activity level were analysed. The stellar parameters and particulars of the observations were discussed in detail in a companion paper that addressed the coronal densities of active stars (TDP04). To the sample analysed in TDP04 we added a set of observations of IM Peg obtained subsequent to the first three segments analysed in Paper I and TDP04; the parameters of these additional observations are listed in Table 1.

Table 1. Parameters of the HETG observations of IM Peg.

Obs ID	Start date and time	$t_{\text{exp}}$ [ks]	$L_X^{\text{a}}$ [erg s $^{-1}$ ]	$L_X^{\text{b}}$ [erg s $^{-1}$ ]
2527	2002-07-01, 15:39:08	24.6	$2.95 \times 10^{31}$	$3.04 \times 10^{31}$
2528	2002-07-08, 02:07:29	24.8	$2.37 \times 10^{31}$	$2.55 \times 10^{31}$
2529	2002-07-13, 06:27:34	24.8	$2.03 \times 10^{31}$	$2.19 \times 10^{31}$
2530	2002-07-18, 21:13:58	23.9	$1.96 \times 10^{31}$	$2.15 \times 10^{31}$
2531	2002-07-25, 11:30:11	23.9	$1.99 \times 10^{31}$	$2.20 \times 10^{31}$
2532	2002-07-31, 20:45:59	22.5	$3.00 \times 10^{31}$	$3.23 \times 10^{31}$
2533	2002-08-08, 00:50:22	23.7	$2.57 \times 10^{31}$	$2.79 \times 10^{31}$
2534	2002-08-15, 14:28:06	23.9	$2.35 \times 10^{31}$	$2.50 \times 10^{31}$

<sup>a</sup>relative to the HEG range: 1.5-15 Å

<sup>b</sup>relative to the MEG range: 2-24 Å

The HETG spectra and the corresponding X-ray lightcurves for the observations can be found in TDP04; we also discuss there the variability observed for some of the stars. The source sample covers very different stellar characteristics, providing a wide view of X-ray emitting stellar coronae; e.g., the X-ray luminosities (in the HETGS bandpasses; see TDP04) span more than five orders of magnitude, from the relatively weak emission of Proxima Centauri with a few  $10^{26}$  erg s $^{-1}$ , up to the very high luminosity ( $\sim 6 \times 10^{31}$  erg s $^{-1}$ ) of the giant HD 223460.

#### 4. Analysis

The data used here were obtained from the *Chandra* Data Archive<sup>4</sup> and have been reprocessed using standard CIAO v3.2.1 tools and analysis threads. Effective areas were calculated using standard CIAO procedures, which include an appropriate observation-specific correction for the time-dependent ACIS contamination layer. Positive and negative spectral orders were summed, keeping HEG and MEG spectra separate. For sources observed in several different segments, we combined the different observations and analysed the coadded spectra. For IM Peg, as noted above, a number of observations are available with which to probe optical depth properties at different times and orbital phases; IM Peg will be discussed in more detail in §5.1.

Spectra were analyzed with the PINTofALE<sup>5</sup> IDL<sup>6</sup> software (Kashyap & Drake 2000) using the technique of spectral fitting described in TDP04. We measured the spectral line intensities of the Ne X Ly $\alpha$  ( $2p^2P_{3/2,1/2} - 1s^2S_{1/2}$ ) and Ly $\beta$  ( $3p^2P_{3/2,1/2} - 1s^2S_{1/2}$ ) transitions from both HEG and MEG spectra, and the O VIII lines from MEG spectra alone (since the latter lie outside the HEG wavelength range).

In order to take into account the mild dependence of the Ly $\alpha$ /Ly $\beta$  ratio on plasma temperature, we also measured the intensities of the Ne IX and O VII resonance line,  $r$  ( $1s2p^1P_1 - 1s^2^1S_0$ ), providing us with an estimate of a representative temperature through the Ly $\alpha$ / $r$  ratio. There are two potential problems with this approach. Firstly, where resonant scattering is relevant, both Ly $\alpha$  and  $r$  transitions can be depleted, and in such a case the Ly $\alpha$ / $r$  ratio might deviate from its expected theoretical behaviour. Secondly, the coronae in which these X-ray lines are formed are expected to be characterised by continuous

---

<sup>4</sup><http://cxc.harvard.edu/cda>

<sup>5</sup><http://hea-www.harvard.edu/PINTofALE>

<sup>6</sup>Interactive Data Language, Research Systems Inc.

ranges of temperatures, rather than by a single, isothermal plasma. However, both of these concerns prove unproblematic.

Figure 2 illustrates the theoretical temperature dependence of the  $\text{Ly}\alpha/r$  ratio and of the  $\text{Ly}\beta/\text{Ly}\alpha$  ratio for Ne lines (O lines show analogous behaviour). The  $\text{Ly}\alpha/r$  is much more temperature-sensitive than  $\text{Ly}\beta/\text{Ly}\alpha$ , and the relatively small deviations from the optically-thin case that might be expected in stellar coronae can only incur small errors in temperature that will have a negligible impact on the predicted  $\text{Ly}\beta/\text{Ly}\alpha$  ratio.

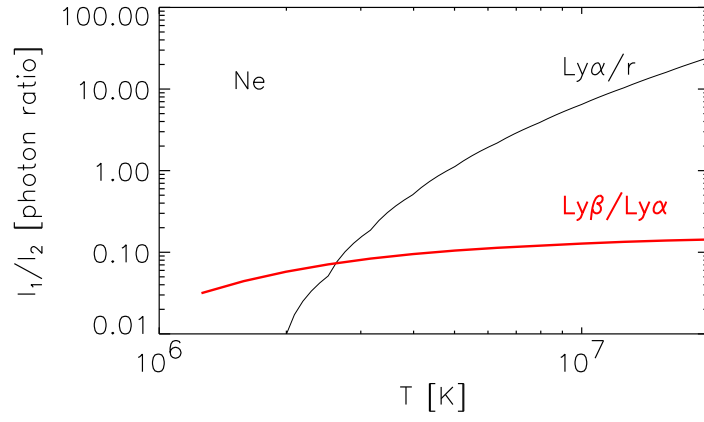


Fig. 2.— Temperature sensitivity (in the isothermal case) of the  $\text{Ly}\alpha/r$  ratio compared to the  $\text{Ly}\beta/\text{Ly}\alpha$  ratio, for neon lines. The corresponding oxygen lines show analogous behaviour.

The accurate temperature determination from the  $\text{Ly}\alpha/r$  ratio strictly holds only for isothermal plasma, whereas stellar coronae are characterised by a thermal distribution of the plasma, so that this diagnostic would give us a temperature weighted by the emission measure distribution (DEM). By computing line ratios for non-isothermal plasma models, and interpreting as if isothermal, we can estimate the errors incurred by an isothermal assumption. We considered two different sets of DEMs: those derived from actual observations of some of the stars in our sample, and simple DEM models in which the emission measure is proportional to  $T^{3/2}$  (as expected for simple hydrostatic loop models; Rosner et al. 1978), or proportional to  $T^{5/2}$  (as observed in some stars such as 31 Com, Scelsi et al. 2004, and reproduced by some hydrodynamic loop models, Testa et al. 2005). For these models we used peak temperatures varying from  $10^{6.5}$  K to  $10^{7.3}$  K. Observed DEMs were culled from the literature for the following sources: AB Dor (Sanz-Forcada et al. 2003b), HD 223460 (Testa et al. 2007), 31 Com,  $\beta$  Cet,  $\mu$  Vel (García-Alvarez et al. 2006), ER Vul, TZ CrB,  $\xi$  UMa (Sanz-Forcada et al. 2003a), 44 Boo (Brickhouse & Dupree 1998), UX Ari (Sanz-Forcada et al. 2002), II Peg (Huenemoerder et al. 2001),  $\lambda$  And (Sanz-Forcada et al. 2002), AR Lac (Huenemoerder et al. 2003), HR 1099 (Drake et al. 2001).

Given the line ratio computed for each DEM model, we inverted the isothermal relation to obtain  $T(\text{Ly}\alpha/r)$ . Using that  $T$ , we then obtained the theoretical isothermal  $\text{Ly}\alpha/\text{Ly}\beta$  ratio ( $\text{Ly}\alpha/\text{Ly}\beta [T(\text{Ly}\alpha/r)]$ ) and compared to the synthetic ratio ( $\text{Ly}\alpha/\text{Ly}\beta [\text{DEM}]$ ). We find that the isothermal assumption is a good predictor of the ratio for both theoretical DEMs and for representative stellar models: Figure 3 shows that the isothermal and DEM ratios are in very good agreement, with differences between the two generally amounting to a few percent. We conclude that the  $\text{Ly}\alpha/r$  temperatures are quite adequate to assess the appropriate expected  $\text{Ly}\alpha/\text{Ly}\beta$  ratio, even if the real plasma temperature distributions of the coronae in our study are far from isothermality.

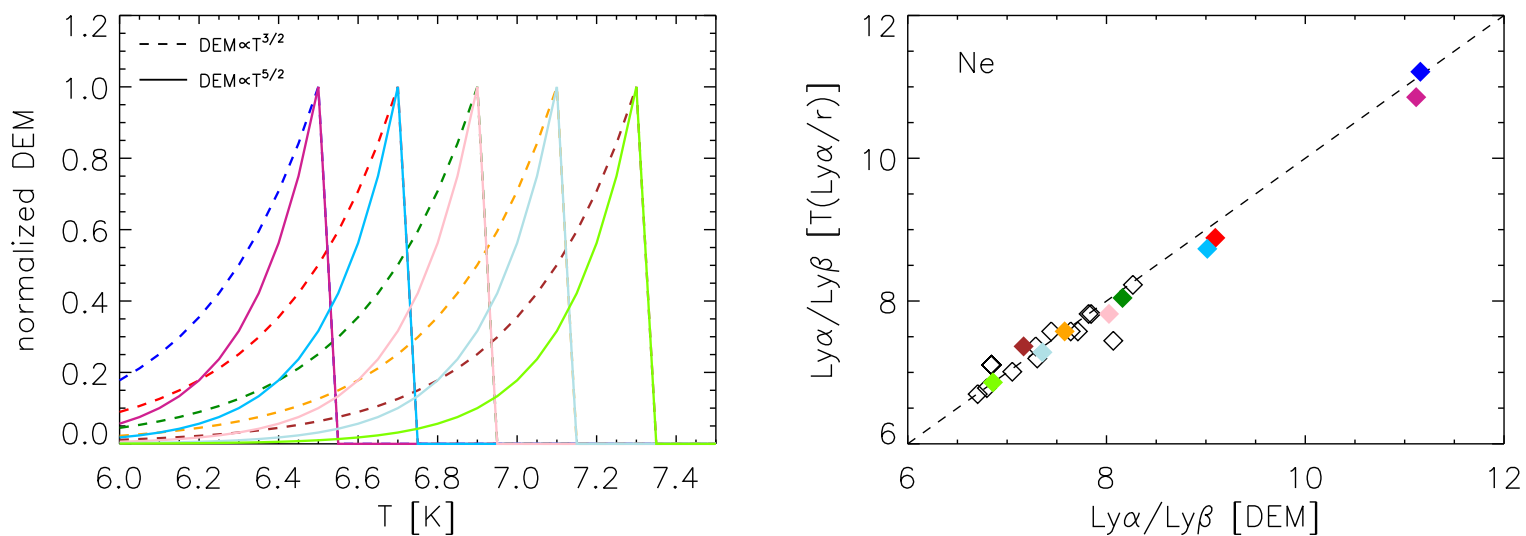


Fig. 3.— *Left panel:* DEM models ( $DEM \propto T^{3/2}, T^{5/2}$ ) used to test the validity of the isothermal approximation. *Right panel:* The Ne x  $Ly\alpha/Ly\beta$  ratios obtained for model (left panel) and observed DEMs (see text; black empty symbols) compared with the  $Ly\alpha/Ly\beta$  ratios expected for isothermal temperatures diagnosed from the DEM Ne  $Ly\alpha/r$  ratios.

#### 4.1. Deblending of Ne X Ly $\alpha$ and O VIII Ly $\beta$

Ne X Ly $\alpha$  and O VIII Ly $\beta$  lines are affected by blending of iron lines unresolved at the HETGS resolution level. Specifically, significant blending is expected for O VIII Ly $\beta$  by an Fe XVIII line ( $2s^22p^4(^3P)3s^2P_{3/2} - 2s^22p^5^2P_{3/2}$ ,  $\lambda = 16.004\text{\AA}$ ), and, to a lesser extent, for the Ne X Ly $\alpha$  line by a nearby Fe XVII transition ( $2s^22p^5(^2P)4d^1P_1 - 2s^22p^6^1S_0$ ,  $\lambda = 12.124\text{\AA}$ ).

**O VIII Ly $\beta$**  — In order to estimate the often significant contribution of Fe XVIII to the O VIII Ly $\beta$  spectral feature, we used the same method described in Paper I, which was also subsequently adopted by Ness & Schmitt (2005) in an analysis of spectra of the classical T Tauri star TW Hya. We estimated the intensity of the  $16.004\text{\AA}$  Fe XVIII line by scaling the observed intensity of the slightly stronger neighbouring unblended Fe XVIII  $16.071\text{\AA}$  ( $2s^22p^4(^3P)3s^4P_{5/2} - 2s^22p^5^2P_{3/2}$ ) transition. Gu (2003b) has recently pointed out the similar behaviour of Fe L-shell lines originating from  $3s$  and  $3p$  upper levels in respect to the indirect excitation processes of radiative recombination, dielectronic recombination, and resonance excitation. The  $16.004\text{\AA}$  and  $16.071\text{\AA}$  transitions originate from similar  $3s$  upper levels and their ratio should therefore not deviate greatly from current theoretical predictions. The APED (v.1.3.1) database (Smith et al. 2001) lists their theoretical ratio as 0.76 at the temperature of the Fe XVIII population peak ( $\sim 6.8$  MK), with a decrease of only a few percent up to 10 MK or so; this range covers the expected formation temperatures of Fe XVIII in our target stars.

We investigated this scaling factor empirically by examining the departure of the resulting deblended Ly $\alpha$ /Ly $\beta$  ratios from the theoretical value as a function of the ratio of the observed Fe XVIII  $16.071\text{\AA}$  to Ly $\beta$  line strengths. If the deblending scaling factor is correct, there should be no residual slope in the resulting data points; a positive slope would instead indicate an over-correction for the blend and a negative slope an under-correction. We found that a slope of zero was obtained for a scaling factor of  $\sim 0.70$ —in good agreement with the APED value within expected uncertainties. This is illustrated in Figure 4.

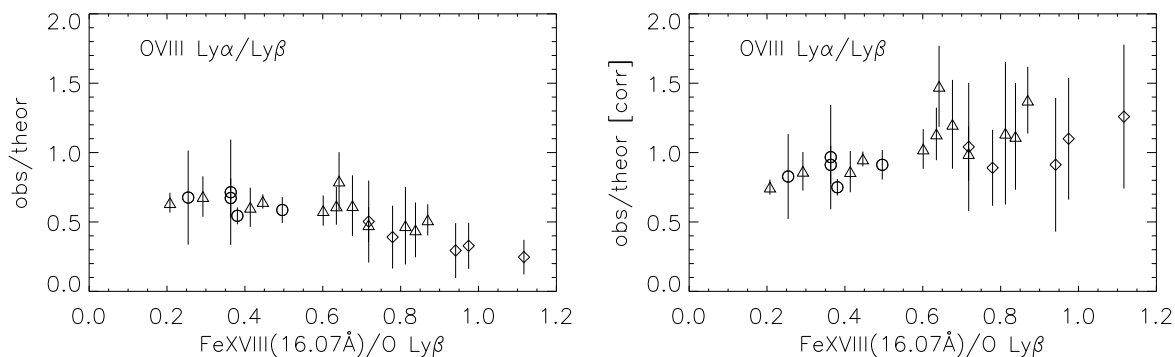


Fig. 4.— O VIII Ly $\alpha$ /Ly $\beta$  ratios (relative to the theoretical ratio) before (*left*) and after (*right*) the correction for the contamination of the Fe XVIII line blending with the O Ly $\beta$  line, plotted vs. the relative intensity of the Fe XVIII line at  $\sim 16.07$  Å and the O Ly $\beta$  before the deblending process. The effect of the blending Fe XVIII line is clear from the *left* plot. The right plot shows the effectiveness of the deblending procedure which eliminates the strong correlation between the departure from the theoretical Ly $\alpha$ /Ly $\beta$  value and the Fe XVIII/O Ly $\beta$  ratio before the deblending.

**Ne X Ly $\alpha$**  — In analogy with the procedure used for the O VIII Ly $\beta$  we searched for isolated and strong Fe XVII lines to estimate the amount of blending from Fe XVII  $\lambda = 12.124\text{\AA}$  in the Ne X Ly $\alpha$  line. A potentially good candidate would be the nearby  $12.266\text{\AA}$  Fe XVII line ( $2s^22p^5(^2P)4d\ ^3D_1 - 2s^22p^6\ ^1S_0$ ), which has a similar intensity and behavior as a function of temperature; however this transition is rather weak in most of the observed spectra, and can be affected itself by blending with a close Fe XXI transition ( $12.284\text{\AA}$ ) barely resolved by HETG.

We therefore chose to use a larger set of Fe XVII lines including stronger transitions. The intensity of the Fe XVII line blending with the Ne X Ly $\alpha$  is estimated by scaling the observed intensity of other Fe XVII lines ( $12.266, 15.014, 15.261, 16.780, 17.051, 17.096\text{\AA}$ ) by the ratio expected from Landi & Gu (2006) (see also Gu 2003a; Landi et al. 2006), assuming  $\log T = 6.8$ . These calculations include indirect processes involving the neighboring charge states, and are quite successful at reproducing the relative intensity of these Fe XVII lines. Previous calculations (including those adopted in APED v.1.3.1) fail here, with, e.g., the ratio of the  $15\text{\AA}$  line to the  $17\text{\AA}$  lines being overestimated by about a factor 2. The detailed comparison of the observed Fe XVII line ratios with the predictions of different theoretical calculations are addressed in a paper in preparation.

The measured line fluxes after application of deblending corrections, together with the statistical errors, are listed in Table 2.

## 5. Results

The observed Ly $\alpha$ /Ly $\beta$  ratios and the temperature derived from the Ly $\alpha$ / $r$  ratios are listed in Table 3 and illustrated in Figure 5. Measurements obtained from the MEG spectra generally result in smaller statistical errors due to the higher S/N; however, we find a general agreement of HEG and MEG results<sup>7</sup>. The main differences of the present work with respect to the analysis of Paper I, where results were presented for 4 sources (II Peg, IM Peg, HR 1099, and AR Lac), are that the line fluxes have been remeasured in the reprocessed data, Ne X

---

<sup>7</sup>The issue of some systematic discrepancies between HEG and MEG measurements has been addressed briefly in TDP04, and it is thoroughly discussed in [http://space.mit.edu/ASC/calib/heg\\_meg/](http://space.mit.edu/ASC/calib/heg_meg/), where systematic discrepancies of 8-10% are found in the 10-12 $\text{\AA}$  range (MEG fluxes being lower than corresponding HEG fluxes at the same wavelength) therefore not significantly affecting the Ly $\alpha$ /Ly $\beta$  ratios. We note that our measured HEG fluxes are in agreement with MEG measurements within  $2\sigma$  for the large majority of cases; the only significant exceptions are the Ne X Ly $\alpha$  of TZ CrB and of HR 1099 ( $3, 5\sigma$  respectively) whose HEG fluxes are  $\sim 10\%$  larger than the corresponding MEG fluxes in agreement with the comparisons presented in [http://space.mit.edu/ASC/calib/heg\\_meg/](http://space.mit.edu/ASC/calib/heg_meg/).

$\text{Ly}\alpha$  fluxes have been corrected for blending, and the deblending procedure for  $\text{O VIII Ly}\beta$  has been slightly refined (see previous section). Also, IM Peg fluxes listed here refer to the total ( $\sim 192$  ks) HETGS spectrum including ObsID 2530-2534 not yet publicly available when we carried out the analysis presented in Paper I (where we used the first three 25 ks pointings; see §5.1 for a detailed discussion).

Table 2. Measured line fluxes (in  $10^{-6}$  photons  $\text{cm}^{-2}$   $\text{s}^{-1}$ ).

Source	Ne					O			Fe	
	$\text{Ly}\alpha^{\text{a}}$ 12.132Å		$\text{Ly}\beta$ 10.239Å		$r$ 13.447Å	$\text{Ly}\alpha$ 18.967Å	$\text{Ly}\beta^{\text{b}}$ 16.006Å	$r$ 21.602Å	$\text{Fe xvii}^{\text{c}}$ 12.124Å	$\text{Fe xviii}$ 16.071Å
	HEG	MEG	HEG	MEG	MEG	MEG	MEG	MEG	MEG	MEG
AU Mic	374 ± 50	356 ± 15	51 ± 10	44 ± 4	208 ± 15	990 ± 40	134 ± 20	243 ± 40	21 ± 5	67 ± 11
Prox Cen	-	69 ± 20	-	6.5 ± 2.9	47 ± 9	306 ± 28	38 ± 14	100 ± 70	6 ± 2	19 ± 13
EV Lac	278 ± 22	262 ± 10	30 ± 6	32 ± 3	209 ± 8	875 ± 19	137 ± 11	330 ± 30	24 ± 5	73 ± 9
AB Dor	668 ± 50	682 ± 24	96 ± 16	86 ± 9	332 ± 27	1400 ± 50	200 ± 22	280 ± 50	41 ± 9	158 ± 16
TW Hya	97 ± 19	95 ± 8	12 ± 8	9.6 ± 2.8	155 ± 14	265 ± 30	38 ± 12	114 ± 40	5.9 ± 2	11 ± 8
HD 223460	158 ± 20	137 ± 11	22 ± 6	16.0 ± 2.7	20 ± 7	229 ± 22	27 ± 11	48 ± 24	10 ± 2	42 ± 10
HD 111812	-	58 ± 5	-	7.9 ± 1.6	14 ± 3	124 ± 16	15 ± 7	40 ± 30	8.8 ± 2	48 ± 5
$\beta$ Cet	419 ± 24	408 ± 10	53 ± 10	48 ± 4	146 ± 10	764 ± 29	62 ± 23	140 ± 40	116 ± 21	426 ± 21
HD 45348	-	54 ± 4	-	4.7 ± 2.3	35 ± 7	127 ± 22	16 ± 8	40 ± 30	11.6 ± 3	30 ± 5
$\mu$ Vel	173 ± 21	159 ± 15	16 ± 13	18 ± 7	95 ± 7	400 ± 30	45 ± 16	46 ± 27	62 ± 12	163 ± 10
Algol	898 ± 50	832 ± 40	136 ± 23	120 ± 8	196 ± 20	1318 ± 50	166 ± 30	190 ± 60	63 ± 14	258 ± 23
ER Vul	218 ± 22	201 ± 12	26 ± 8	24.3 ± 2.8	74 ± 7	362 ± 29	39 ± 12	66 ± 40	24 ± 5	88 ± 9
44 Boo	572 ± 60	537 ± 24	75 ± 11	68 ± 8	254 ± 20	1450 ± 60	122 ± 22	266 ± 60	53 ± 11	151 ± 16
TZ CrB	1126 ± 30	1043 ± 24	145 ± 14	127 ± 6	516 ± 20	2110 ± 50	178 ± 26	300 ± 50	131 ± 25	445 ± 20
UX Ari	730 ± 40	767 ± 20	126 ± 17	107 ± 8	245 ± 18	926 ± 50	147 ± 21	158 ± 40	14.5 ± 3	55 ± 13
$\xi$ UMa	419 ± 27	394 ± 13	42 ± 8	47 ± 4	309 ± 16	1510 ± 60	169 ± 22	496 ± 60	83 ± 17	185 ± 15
II Peg	1300 ± 70	1200 ± 30	183 ± 24	191 ± 10	356 ± 20	1950 ± 70	350 ± 30	250 ± 50	18 ± 4	86 ± 16
$\lambda$ And	557 ± 30	556 ± 14	80 ± 11	84 ± 5	189 ± 14	984 ± 40	113 ± 17	110 ± 30	24.6 ± 6	137 ± 12
TY Pyx	341 ± 29	312 ± 6	46 ± 12	40 ± 5	142 ± 15	468 ± 50	51 ± 21	96 ± 50	25 ± 5	106 ± 17
AR Lac	648 ± 40	621 ± 17	104 ± 15	94 ± 6	182 ± 20	888 ± 50	94 ± 23	130 ± 50	34 ± 7	129 ± 14
HR 1099	1960 ± 40	1730 ± 18	255 ± 14	230 ± 7	566 ± 18	2680 ± 50	367 ± 21	410 ± 40	58 ± 12	246 ± 14
IM Peg	408 ± 25	383 ± 10	62 ± 7	60 ± 3	79 ± 8	490 ± 30	75 ± 12	50 ± 20	10.6 ± 2.5	45 ± 8

<sup>a</sup>Ne  $\text{Ly}\alpha$  fluxes after the deblending with the Fe xvii line at 12.124Å.

<sup>b</sup>O  $\text{Ly}\beta$  fluxes after the deblending with the Fe xviii line at 16.004Å.

<sup>c</sup>Fe xvii line (at 12.124Å) flux estimated by scaling the measured fluxes of the other Fe xvii lines.

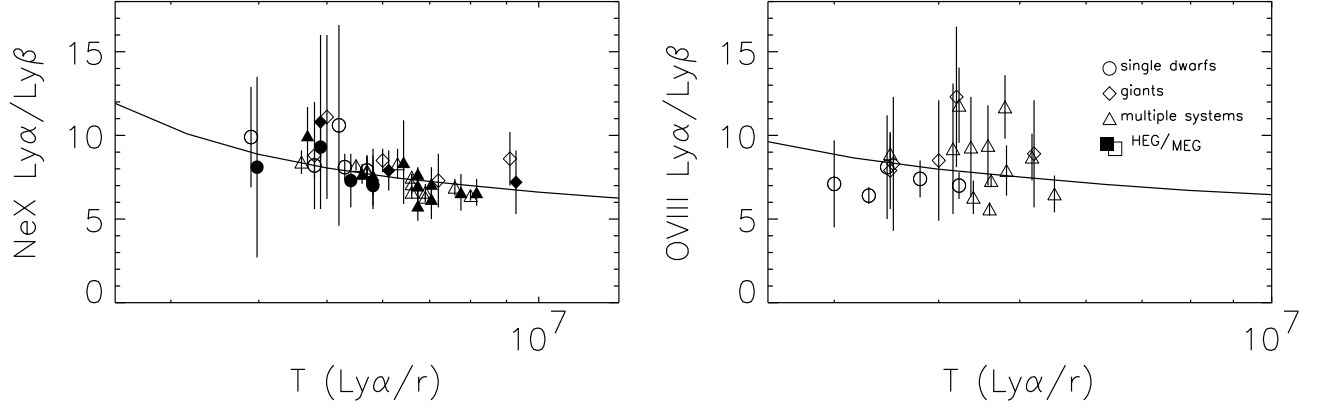


Fig. 5.—  $\text{Ly}\alpha/\text{Ly}\beta$ , both from HEG (filled symbols) and from MEG (empty symbols) vs. temperature, as derived from the ratio of the  $\text{Ly}\alpha$  and the He-like resonance line. The solid line mark the theoretical ratio from APED, expected for isothermal plasma at the corresponding temperature. As indicated on the right plot, different symbols are used for different classes of sources.  $\text{Ly}\alpha/\text{Ly}\beta$  ratios from HEG are shifted in  $T$  by 2% to separate them from the MEG measurements.

Table 3. Ly $\alpha$ /Ly $\beta$  photon ratios and plasma temperature, with  $1\sigma$  errors.

Source	Ne					O		
	$T^a$	Ly $\alpha$ /Ly $\beta$		$\Delta[\sigma]^b$		$T^a$	Ly $\alpha$ /Ly $\beta$	$\Delta[\sigma]^b$
	[10 <sup>6</sup> K]	HEG	MEG	HEG	MEG	[10 <sup>6</sup> K]	MEG	MEG
AU Mic	5.3 <sup>+0.2</sup> <sub>-0.1</sub>	7.3 ± 1.6	8.1 ± 0.8	-0.4	0.1	3.8 <sup>+0.2</sup> <sub>-0.2</sub>	7.4 ± 1.1	-0.7
Prox Cen	5.2 <sup>+0.5</sup> <sub>-0.7</sub>	...	10.6 ± 6	...	0.4	3.5 <sup>+0.7</sup> <sub>-0.9</sub>	8.1 ± 3.1	-0.1
EV Lac	4.8 <sup>+0.1</sup> <sub>-0.1</sub>	9.3 ± 1.9	8.2 ± 0.8	0.5	-0.1	3.3 <sup>+0.1</sup> <sub>-0.2</sub>	6.4 ± 0.5	-4
AB Dor	5.7 <sup>+0.1</sup> <sub>-0.2</sub>	7.0 ± 1.3	7.9 ± 0.9	-0.6	0.3	4.2 <sup>+0.2</sup> <sub>-0.4</sub>	7.0 ± 0.8	-0.9
TW Hya	3.9 <sup>+0.1</sup> <sub>-0.1</sub>	8.1 ± 5.6	9.9 ± 3.0	-0.1	0.3	3.0 <sup>+0.3</sup> <sub>-0.4</sub>	7.1 ± 2.6	-0.7
HD 223460	9.1 <sup>+1.3</sup> <sub>-1.5</sub>	7.2 ± 2.1	8.6 ± 1.6	0.3	1.2	4.0 <sup>+0.8</sup> <sub>-0.8</sub>	8.5 ± 3.6	0.2
HD 111812	7.2 <sup>+0.7</sup> <sub>-0.6</sub>	...	7.3 ± 1.6	...	0.1	3.5 <sup>+0.7</sup> <sub>-1.2</sub>	8.3 ± 4.0	0
$\beta$ Cet	6.0 <sup>+0.2</sup> <sub>-0.1</sub>	7.9 ± 1.5	8.5 ± 0.7	0.2	1.2	4.2 <sup>+0.6</sup> <sub>-0.4</sub>	12.3 ± 4.2	1.0
HD 45348	5.0 <sup>+0.2</sup> <sub>-0.5</sub>	...	11.2 ± 5.4	...	0.6	3.5 <sup>+0.9</sup> <sub>-1.3</sub>	7.9 ± 2.3	-0.2
$\mu$ Vel	4.8 <sup>+0.2</sup> <sub>-0.2</sub>	10.8 ± 6.8	8.8 ± 3.5	0.4	0.1	5.2 <sup>+1.0</sup> <sub>-1.6</sub>	8.9 ± 3.2	0.5
Algol	7.6 <sup>+0.4</sup> <sub>-0.4</sub>	6.6 ± 1.2	6.9 ± 0.6	-0.4	-0.3	4.8 <sup>+0.3</sup> <sub>-0.8</sub>	7.9 ± 1.5	0.2
ER Vul	6.3 <sup>+0.1</sup> <sub>-0.3</sub>	8.4 ± 2.7	8.3 ± 1.1	0.3	0.8	4.4 <sup>+0.8</sup> <sub>-1.4</sub>	9.3 ± 3.0	0.5
44 Boo	5.7 <sup>+0.1</sup> <sub>-0.2</sub>	7.6 ± 1.4	7.9 ± 1.0	-0.1	0.2	4.2 <sup>+0.4</sup> <sub>-0.4</sub>	11.9 ± 2.2	1.9
TZ CrB	5.5 <sup>+0.2</sup> <sub>-0.1</sub>	7.7 ± 0.8	8.2 ± 0.4	-0.1	0.9	4.8 <sup>+0.2</sup> <sub>-0.4</sub>	11.9 ± 1.8	2.2
UX Ari	6.6 <sup>+0.3</sup> <sub>-0.1</sub>	5.8 ± 0.9	7.1 ± 0.6	-1.7	-0.3	4.4 <sup>+0.4</sup> <sub>-0.4</sub>	6.3 ± 1.0	-1.3
$\xi$ UMa	4.6 <sup>+0.2</sup> <sub>-0.1</sub>	10.0 ± 2.0	8.4 ± 0.8	0.8	0.0	3.5 <sup>+0.1</sup> <sub>-0.2</sub>	8.9 ± 1.2	0.4
II Peg	6.9 <sup>+0.3</sup> <sub>-0.1</sub>	7.1 ± 1.0	6.3 ± 0.4	-0.2	-2.8	4.6 <sup>+0.4</sup> <sub>-0.4</sub>	5.6 ± 0.4	-5
$\lambda$ And	6.6 <sup>+0.1</sup> <sub>-0.3</sub>	7.0 ± 1.0	6.6 ± 0.4	-0.4	-1.8	5.2 <sup>+0.5</sup> <sub>-0.6</sub>	8.7 ± 1.4	0.9
TY Pyx	5.7 <sup>+0.3</sup> <sub>-0.2</sub>	7.4 ± 1.8	7.8 ± 0.9	-0.1	0.1	4.2 <sup>+0.6</sup> <sub>-1.0</sub>	9.2 ± 3.9	0.4
AR Lac	6.9 <sup>+0.3</sup> <sub>-0.3</sub>	6.2 ± 1.1	6.6 ± 0.6	-1.0	-1.2	4.6 <sup>+0.6</sup> <sub>-0.8</sub>	9.4 ± 2.4	0.8
HR 1099	6.6 <sup>+0.1</sup> <sub>-0.1</sub>	7.7 ± 0.4	7.5 ± 0.2	0.7	0.5	4.6 <sup>+0.2</sup> <sub>-0.2</sub>	7.3 ± 0.4	-0.6
IM Peg	8.0 <sup>+0.4</sup> <sub>-0.3</sub>	6.6 ± 0.8	6.4 ± 0.3	-0.5	-1.8	5.5 <sup>+0.8</sup> <sub>-1.1</sub>	6.5 ± 1.1	-0.8

<sup>a</sup> $T$  derived from the Ly $\alpha$ / $r$  line ratio diagnostics.

<sup>b</sup>Discrepancy between Ly $\alpha$ /Ly $\beta$  measured and theoretical value in units of  $\sigma$ .

The observed Ne X Ly $\alpha$ /Ly $\beta$  ratios follow closely the APED theoretical predictions as a function of temperature. The values for the O VIII ratios (right panel of Fig. 5) show slightly more scatter, with some departures below theory and some 1-2 $\sigma$  excursions above. We note that an *enhancement* of the Ly $\alpha$ /Ly $\beta$  ratio is possible for the particular geometry in which an emitting region is optically-thick in some directions but is optically-thin in the line-of-sight of the observer (see also the radiative transfer study of Kerr et al. 2004). Such a situation is disfavoured by the isotropic nature of the scattering process in which any line enhancements through scattering are diluted, roughly speaking, by the ratio of solid angles of optically-thin to optically-thick lines-of-sight. In the case of loop geometries, such a ratio is much larger than unity. We therefore interpret these small upward 1-2  $\sigma$  excursions as normal statistical fluctuations.

In the case of the Ne X lines, the MEG Ly $\alpha$ /Ly $\beta$  ratio for II Peg is  $\sim 3\sigma$  lower than the expected value; the ratio derived from HEG is consistent with the MEG measurement but does not depart significantly from theory. The only sources showing O VIII Ly $\alpha$ /Ly $\beta$  significantly ( $> 3\sigma$ ) lower than the theoretical ratio are II Peg and EV Lac. We note that the low Ly $\alpha$ /Ly $\beta$  ratios for IM Peg discussed in Paper I were found in the spectra obtained in the first three pointings while here we analyze the whole set of observations; in §5.1 below we discuss the variability observed in Ly $\alpha$ /Ly $\beta$  ratios for IM Peg.

One other interesting case is the T Tauri star, TW Hya, that shows very high density,  $n_e \gtrsim 10^{12} \text{ cm}^{-3}$ , at the temperature of O VII lines (e.g., Kastner et al. 2002). In this case, the high densities are generally believed to arise from an accretion shock, rather than coronal loops; significant scattering effects could in principle provide interesting constraints on the dimensions of the shock region. Unfortunately, for this source the relatively low S/N results in large error bars in the Ly $\alpha$ /Ly $\beta$  ratios that do not provide any useful constraints (as was also noted in the analysis of Fe XVII lines by Ness & Schmitt 2005).

## 5.1. IM Peg

The different *Chandra* HETG observations of the RS CVn system IM Peg provide an opportunity for studying the optical depth and its possible variation with time. This system has been analyzed in great detail at optical wavelengths by Berdyugina et al. (1999, 2000). These works depict a scenario with stellar spots concentrated mainly close to the polar regions, similar to those found for many other active systems (e.g., Schuessler et al. 1996; Hatzes et al. 1996; Vogt et al. 1999; Hussain et al. 2002; Berdyugina et al. 1998).

*Chandra* observed IM Peg eight times over  $\sim 2$  orbital periods (see Tab. 1). The X-ray lightcurve obtained from this sequence is illustrated in Figure 6 and shows significant modulation that is possibly related to the orbital and rotational period (these being essentially the same;  $P_{\text{rot}} = 24.39$  d,  $P_{\text{orb}} = 24.65$  d, Strassmeier et al. 1993). In Paper I we analyzed the first three 25 ks HETGS observations of IM Peg, publicly available at that time, and we found remarkably small photon path lengths based on optical depth effects. The compact emission regions implied might be associated with active regions revealed by optical Doppler imaging studies. Any significant net line photon loss to resonant scattering out of the line-of-sight would be expected to be sensitive to the orientations of the emitting structures. Modulation of the  $\text{Ly}\alpha/\text{Ly}\beta$  ratio with time could provide important new structure and morphology diagnostics. Such regions might also be expected to change on relatively short timescales as a result of flaring activity and consequent re-alignment of their defining magnetic fields.

Table 4.  $\text{Ly}\alpha/\text{Ly}\beta$  photon ratios with  $1\sigma$  errors.

Obs. ID	Ne x		O VIII
	HEG	MEG	MEG
2527+2528	$5.3 \pm 0.8$	$5.5 \pm 0.5$	$5.1 \pm 1.2$
2529+2530+2531	$6.9 \pm 1.7$	$6.5 \pm 0.6$	$7.5 \pm 3.0$
2532+2533+2534	$6.2 \pm 1.2$	$7.1 \pm 0.6$	$7.0 \pm 2.1$

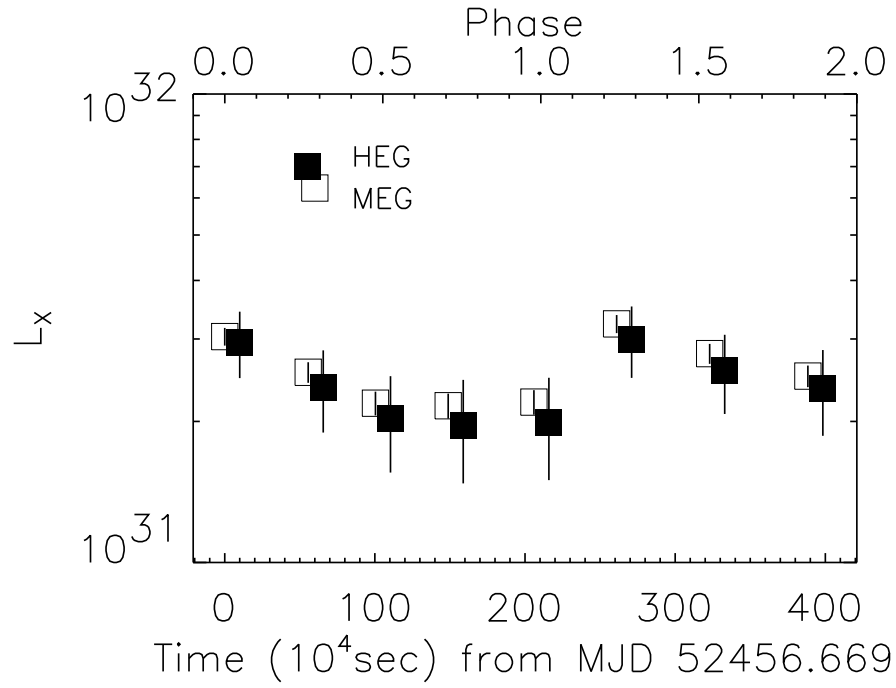


Fig. 6.— Lightcurve of IM Peg *Chandra* observations; both HEG (*filled squares*) and MEG (*empty squares*)  $L_X$  are presented. HEG values are shifted by  $10^5$  s on the time axis with respect to the corresponding MEG measurements. The phases corresponding to the absolute times are indicated at the top of the plot.

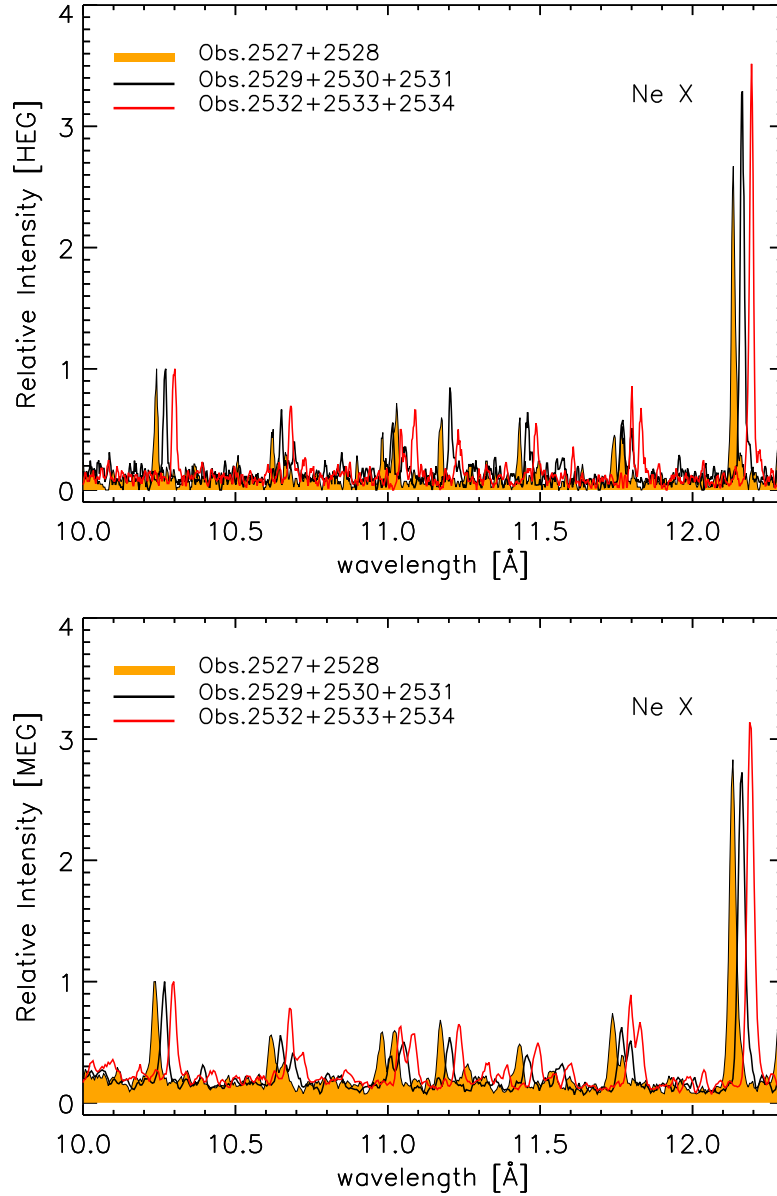


Fig. 7.— Ne X Ly $\alpha, \beta$  spectral region for the three chosen time segments of the observation of the RS CVn system IM Peg, as indicated in the plots. Both HEG (*upper panel*) and MEG (*lower panel*) spectra are presented, normalized to the intensity of the Ly $\beta$  line at 10.24 Å. For better readability the spectra corresponding to the second (2529+2530+2531) and the third (2532+2533+2534) segment are shifted in wavelength with respect to the first (2527+2528) by +0.03 Å and +0.06 Å respectively. Note the pronounced difference in Ly $\alpha$  and Ly $\beta$  relative intensity in the three spectra especially between the first and the third spectra.

Here we present an analysis of the complete dataset, exploring possible temporal variability of the optical depth of the coronal plasma. Unfortunately, the single IM Peg exposures provided counts sufficient for reliable intensity measurement only for the strongest lines in the spectrum, such as Ne X Ly $\alpha$ . In order to probe secular change in the Ly $\alpha$ /Ly $\beta$  ratio, we therefore measured lines from spectra coadded from contiguous sets of two or three observations that sample different phases of the stellar period: ObsIDs 2527 and 2528; 2529, 2530, and 2531; and 2532, 2533, and 2534. The spectra in the Ne and O Ly $\alpha, \beta$  regions for these three portions of the observation are shown in Figure 7 and 8. The measured Ly $\alpha$ /Ly $\beta$  ratios are listed in Table 4.

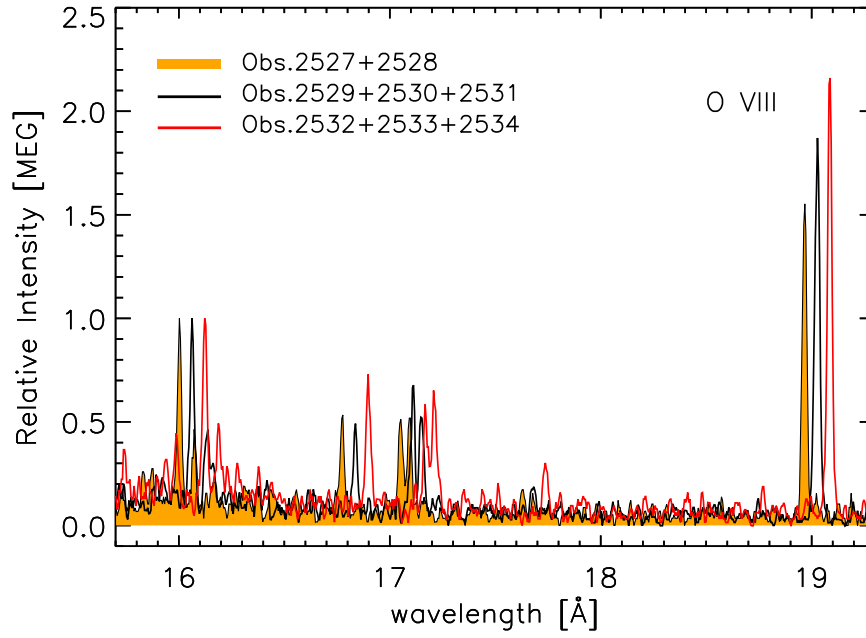


Fig. 8.— O VIII Ly $\alpha$ , $\beta$  spectral region of MEG spectra of IM Peg for the three chosen time segment of the observation, in the same format of the plots in Figure 7. The shift in wavelength of second and third spectra is of +0.06 Å with respect to the preceding spectrum. A clear trend in the Ly $\alpha$ /Ly $\beta$  line ratio is present.

The  $\text{Ly}\alpha/\text{Ly}\beta$  ratios, while statistically all consistent with one another, are suggestive of different conditions in the different portions of the observation. Both Ne and O  $\text{Ly}\alpha/\text{Ly}\beta$  ratios in HEG and MEG spectra are lower than the corresponding APED theoretical value in the first segment, as already discussed in Paper I and noted earlier. The rest of the observation is characterized by  $\text{Ly}\alpha/\text{Ly}\beta$  values compatible with theory. The measured ratios are illustrated as a function of the hardness ratio ( $HR = (H - S)/(H + S)$ , where  $H$  is the flux integrated in the 2-9Å wavelength band, and  $S$  is the flux integrated in the 9-25Å band) in the different segments of the observation in Figure 9. There is no obvious correlation of  $\text{Ly}\alpha/\text{Ly}\beta$  with spectral hardness that might suggest, e.g., that the former changes as a result of plasma temperature changes. These results show that it might be worthwhile to explore, when the data quality allows it, temporal variability of optical depth properties in stellar coronae, expected to some extent on the basis of their dependence on the line-of-sight and coronal geometry other than on the physical conditions of the emitting plasma.

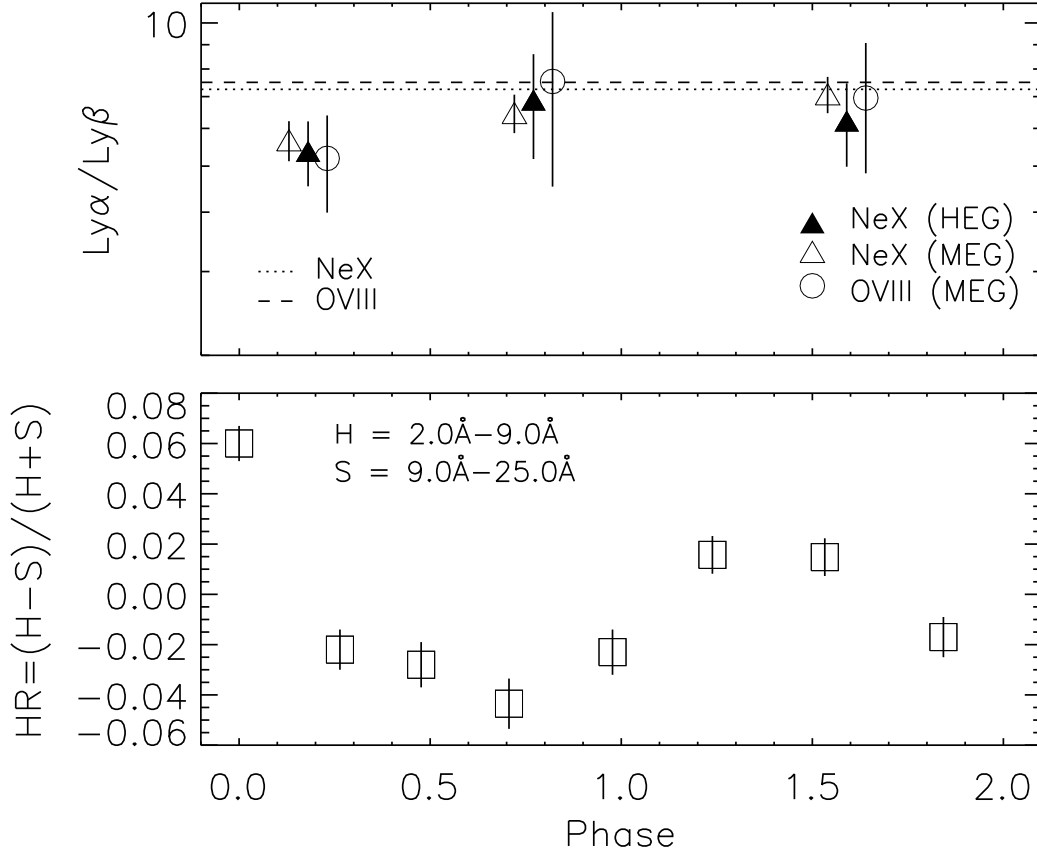


Fig. 9.—  $Ly\alpha/Ly\beta$  ratios measured from IM Peg spectra for the three time segments selected for the analysis (2528+2528, 2529+2530+2531, and 2532+2533+2534; *upper panel*), together with the hardness ratio, HR (*lower panel*). In the *upper panel* the horizontal lines represent the APED values expected for the  $Ly\alpha/Ly\beta$  ratio of O (*dashed line*) for a temperature of 5 MK, and of Ne (*dotted line*) for a temperature of 9 MK. For better readability  $Ly\alpha/Ly\beta$  ratios of Ne X from HEG, and of O VIII are shifted with respect to MEG Ne X  $Ly\alpha/Ly\beta$  ratios by +0.05 and +0.1 respectively on the phase axis.

## 5.2. Path length estimates

The data presenting more reliable evidence for optical thickness are the spectra of IM Peg from the first two observations, where Ly $\alpha$  of both oxygen and neon appear to be depleted with respect to the corresponding Ly $\beta$  transition (deviation of  $\sim 1.8\sigma$  and  $\sim 3\sigma$  respectively), and the spectrum of II Peg characterized by an O VIII Ly $\alpha$ /Ly $\beta$  ratio  $\sim 5\sigma$  lower than the theoretical value. As pointed out in Paper I, the discrepancies between observed and theoretical Ly $\alpha$ /Ly $\beta$  line strength ratios in IM Peg and II Peg cannot be explained by photoelectric absorption along the line-of-sight on the basis of their measured H column densities (Mewe et al. 1997; Mitrou et al. 1997). It is worth discussing whether these transitions, and in particular their ratios, might be affected by non-equilibrium conditions that are possibly relevant for these active stars undergoing frequent flaring activity. Non-equilibrium effects might be responsible for changes in the O VII  $G$  ratio  $((f + i)/r)$  observed for EV Lac between quiescent and flare phases (Mitra-Kraev 2006). It is well-known that the  $G$  ratio is sensitive to deviations from coronal equilibrium, because recombination processes contribute significantly to  $f$  and  $i$  but are almost negligible for  $r$  (e.g. Pradhan 1985). Even though recombination processes have non-negligible effects on Ly $\alpha$  and Ly $\beta$  (10-15%), they contribute to a very similar extent to the two transitions, and therefore their ratio is not expected to change significantly under mildly non-equilibrium conditions. Furthermore, we note that for the typical conditions of the coronal plasma in these active stars the expected timescales of these effects are only of the order of hundreds of seconds (e.g., Golub et al. 1989), i.e. very short with respect to our integration times of several tens of kiloseconds. We therefore interpreted the discrepant ratios in terms of a relative depletion of the Ly $\alpha$  line flux due to resonance scattering processes.

Another source apparently showing significant effects of resonant scattering is EV Lac, whose O VIII Ly $\alpha$ /Ly $\beta$  ratio is more than  $3\sigma$  lower than the corresponding theoretical value. This result is supported to some extent by the findings of Ness et al. (2003): in their survey of coronal optical depth properties based on the analysis of Fe XVII transitions, EV Lac is the only source deviating significantly from the typical values found for all other coronae. However, Ness et al. (2003) did not consider this result robust due to discrepancies between HEG and MEG measurements.

For the stars with Ly $\alpha$ /Ly $\beta$  departing from the theoretical values we can derive an estimate of the photon path length using the Kaastra & Mewe (1995) approximation to the escape probability formalism of Kastner & Kastner (1990), as described in § 3.1 of Paper I. The observed Ly $\alpha$ /Ly $\beta$  can be expressed in terms of the line center optical depths  $\tau^k$ , f-values

$f^k$ , and photon pathlength  $\ell$ , as

$$\frac{(I_{Ly\alpha}/I_{Ly\beta})_{\text{obs}}}{(I_{Ly\alpha}/I_{Ly\beta})_{\text{th}}} = \frac{1}{3} \left[ \frac{2}{1 + 0.43C(\ell)f_1^\alpha} + \frac{1}{1 + 0.43C(\ell)f_1^\alpha/2} \right] \cdot (1 + 0.43C(\ell)f^\beta) \quad (2)$$

where  $C(\ell) \cdot f^k = \tau^k$  and the line center optical depth is given by

$$\tau = 1.16 \cdot 10^{-14} \cdot \frac{n_i}{n_{\text{el}}} A_Z \frac{n_{\text{H}}}{n_{\text{e}}} \lambda f \sqrt{\frac{M}{T}} n_{\text{e}} \ell \quad (3)$$

where  $n_i/n_{\text{el}}$  is the ion fraction (from Mazzotta et al. 1998),  $A_Z$  is the element abundance,  $n_{\text{H}}/n_{\text{e}} \sim 0.85$ ,  $f$  is the oscillator strength,  $M$  the atomic weight,  $T$  the temperature, and  $n_{\text{e}}$  the electron density. The Ly $\alpha$  and Ly $\beta$  f-values are  $f_1^\alpha = 0.2776$ , and  $f_1^\beta = 0.05274$  (e.g. Morton 2003).

We use the electron densities,  $n_{\text{e}}$ , derived from the diagnostics of the He-like triplets TDP04. The coronal abundances assumed for II Peg and IM Peg are discussed in Paper I; for EV Lac we assume O/H=8.40, as derived by Favata et al. (2000b), expressed on the usual spectroscopic logarithmic scale in which X/H=  $\log[n(\text{X})/n(\text{H})] + 12$ , where  $n(\text{X})$  is the number density of element X.

In Table 5 we list the values obtained for the path length estimates,  $\ell_\tau$ , and for comparison, we list the stellar radii and loop lengths expected for a standard hydrostatic loop model (e.g. Rosner et al. 1978, RTV hereafter) corresponding to the observed temperatures and densities.

Table 5. Path length derived from measured Ly $\alpha$ /Ly $\beta$  ratios.

Source		$\ell_\tau$ [cm]	$L_{\text{RTV}}^{\text{a}}$ [cm]	$\ell_\tau/R_\star^{\text{b}}$	$f_s^{\text{c}}$	$E_S^{\text{d}}$ [erg cm $^{-2}$ s $^{-1}$ ]
IM Peg	O VIII	$1.5 \cdot 10^{10}$	$2.2 \cdot 10^9$	0.017	$\sim 0.006$	$\sim 7.2 \cdot 10^7$
	Ne X [HEG]	$2.1 \cdot 10^8$	$2.8 \cdot 10^7$	0.00024	$\sim 0.0003$	$\sim 5.2 \cdot 10^{10}$
	Ne X [MEG]	$1.7 \cdot 10^8$	$2.8 \cdot 10^7$	0.00019	$\sim 0.0004$	$\sim 5.3 \cdot 10^{10}$
II Peg	O VIII	$9.5 \cdot 10^9$	$1 \cdot 10^9$	0.04	$\sim 0.021$	$\sim 1.2 \cdot 10^8$
EV Lac	O VIII	$1.6 \cdot 10^9$	$2.6 \cdot 10^8$	0.058	$\sim 0.016$	$\sim 1.9 \cdot 10^8$

<sup>a</sup>Loop length from RTV scaling laws:  $L_{\text{RTV}} \sim T^3/[(1.4 \times 10^3)^3 \cdot p]$ .

<sup>b</sup>Path length as fraction of the stellar radius.

<sup>c</sup>Coronal surface filling factor, defined as  $f_s = A/A_\star = (V/\ell_\tau)/A_\star = [EM/(n_e^2 \ell_\tau)]/A_\star$ .

<sup>d</sup>Estimate of surface heating flux (see text for details).

## 6. Discussion

This work presents a detailed and extensive study of the O VIII and Ne X Ly $\alpha$ /Ly $\beta$  ratios in a sample of active stars, paying careful attention to the presence of blends and to the validity of theoretical line ratio predictions. Our analysis shows that optical depth effects are generally negligible in the disk-integrated X-ray spectra emitted by stellar coronae over a wide range of activity, in line with previous studies based on Fe XVII lines (e.g., Ness et al. 2003; Audard et al. 2004). We argued in §2 that the coronal abundance patterns exhibited by most active stars renders the Ne and O Lyman lines more sensitive diagnostics of optical depth than the Fe lines, and in this regard our study extends the results of previous surveys.

However, our study has also yielded convincing indication of line-of-sight photon loss through resonant scattering in the spectra of three stars, IM Peg, II Peg and EV Lac. The detection of significant X-ray optical depth is particularly interesting, because it provides us with insights into the characteristic dimensions of the emitting coronal structures.

Before proceeding, we note here that a simple escape probability analysis does not include the scattering source term itself, and so photons scattered *into* the line of sight that could enhance the observed line strength are not included. For instance, in the case of a spherically symmetric corona in which the line optical depth were significant, scattering into and out of the line of sight would be balanced and line strengths not affected (see e.g., Wood & Raymond 2000). Strictly, then, the photon path,  $\ell$ , entering into the equations in §5.2 should be interpreted as a *lower limit* to the true photon path length. This is potentially important. Phillips et al. (2001), for example, used the lack of appreciable depletion of the Fe XVII resonant line at  $\sim 15.01\text{\AA}$  to deduce an upper limit of 3000 km for size of emitting regions in the corona of Capella; however, such a measurement in reality only provides an *upper limit to the lower limit*, therefore not providing a constraint. Indeed, the lack of evidence for line quenching through scattering in most of our sample stars does not imply that scattering is not a significant source term, but merely that the scattering geometry is such that there is no net loss or gain of photons in the line-of-sight.

Instead, a positive detection of resonance scattering has interesting implications and points to a non-uniform “aspect ratio” of the dominant coronal emitting regions: for any net line depletion to occur, an emitting structure must generally be more elongated along the line of sight than in the perpendicular direction. In the context of a corona comprising plasma contained by magnetic loops, there are different ways in which this can be interpreted: (1) scattering loss results from the structure and viewing angle of the loops themselves; (2) scattering loss arises because of a particular conglomeration of loops viewed at a particular angle. Each case leads to fundamentally different interpretations of observed scattering. In the former case, a loop with random orientation must generally be viewed from the top, in

which direction the photon path length through the plasma is largest. Photon loss through resonance scattering then implies that loops are preferentially placed on the stellar surface facing the observer (a perfect alignment of loops seen edge-on on the stellar limb could produce a similar effect, though such a chance alignment is unlikely). In the latter case, the coronal structures or active regions must be placed preferentially on the stellar limb.

### 6.1. Scattering within individual loops

With the proviso that a scattering-derived path length is a lower limit to the true emitting region size, we note that the photon path lengths implied by the analysis of line ratios (§5.2) observed in II Peg, IM Peg and EV Lac and listed in Table 5 are all much smaller than the corresponding stellar radii, but are also about an order of magnitude *larger* than expected from RTV loops.

Under the assumption that scattering within individual loops arises when they are viewed from the top, we can interpret the path length estimates,  $\ell_\tau$ , in terms of the coronal scale height. With knowledge of the total emitting volume we can also derive an estimate of the surface filling factors. Emitting volumes can be estimated using the emission measures implied by the different lines,  $V = EM/n_e^2$ , combined with electron densities,  $n_e$ , derived in TDP04. The surface filling factors,  $f_s$ , are then given by  $f_s = A/A_\star = (V/\ell_\tau)/A_\star$ . The derived filling factors, listed in Table 5, are very small, and especially so for the hotter plasma. They are also an order of magnitude smaller than those previously derived in TDP04 based on RTV loops—a direct consequence of the optical depth scale height being commensurately larger than those suggested by simple quasi-static loop models.

The small filling factors we find here have interesting implications for the surface heating flux requirements. A very rough estimate of the heating required to sustain the observed physical conditions of the plasma can be obtained from the RTV scaling laws. While our estimated loop lengths are significantly longer than suggested by RTV models, these relations should still suffice for the purposes of estimation. The volumetric heating per unit time,  $E$ , is given by  $E \sim 10^5 \cdot p^{7/6} L^{-5/6}$ , where  $p$  is the plasma pressure and  $L$  the loop length. By assuming  $L = \ell_\tau$  we find for the the surface flux values of order of  $10^8$  erg cm<sup>-2</sup> s<sup>-1</sup> for O VIII lines, and several  $10^{10}$  erg cm<sup>-2</sup> s<sup>-1</sup> implied by the Ne X lines in IM Peg (Table 5). These compare with typical surface heating rates for the cores of solar active regions of a few  $10^7$  erg cm<sup>-2</sup> s<sup>-1</sup> (e.g., Withbroe & Noyes 1977).

In the comparison of  $\ell_\tau$  with  $L_{\text{RTV}}$  we assumed to some extent that  $\ell_\tau$  is a reasonable estimate for the coronal scale height (i.e. for the loop length). However, an alternative

interpretation is possible in which the actual coronal loops are larger and  $\ell_\tau$  represents only an estimate of the length of the part of the loop containing plasma at the characteristic temperature of the quenched lines. In such a scenario, the values found for  $\ell_\tau$  can suggest the presence of cooler loops with maximum temperature around 3 MK, similar to solar loops, coexistent with loops with much higher maximum temperature ( $\gtrsim 10$  MK). In these hotter loops, the plasma emitting the Ne X lines ( $T \gtrsim 6\text{--}7$  MK) would be confined in the lower portion of the loop, which is characterized by higher density. In order to estimate the region of the loop occupied by the plasma emitting the observed line,  $\Delta l$ , we can use the equations for the conductive flux:

$$F_c = k_c T^{5/2} \cdot dT/dl \sim k_c T^{5/2} \cdot \Delta T/\Delta l; \quad (4)$$

and from RTV relations for a radiative power loss function  $P(T)$ :

$$F_c/\Delta l \sim n_e^2 P(T). \quad (5)$$

Assuming  $T$  is the temperature of maximum formation of the line  $k$ ,  $T_{\max}^k$ , and  $\Delta T$  is the width in temperature of the line emissivity curve ( $\sim 0.3$  dex), we can solve the equations for  $\Delta l$ :

$$\Delta l \sim 5 \cdot 10^8 \text{ cm for O VIII}$$

$$\Delta l \sim 2 \cdot 10^7 \text{ cm for Ne X}$$

The resulting values of  $\Delta l$  are rather close to  $L_{RTV}$  (see Table 5), obtained assuming  $T_{\max}^k$  as maximum temperature of the loop, and are still much smaller than  $\ell_\tau$ . We can conclude then, that the values derived for the path length do not seem to agree with the hypothesis of standard uniformly heated quasi-static loop models.

## 6.2. Scattering within active regions

The maximum path length,  $l_{\max}$ , through a spherically-symmetric corona of height  $h$  on a star with radius  $R_\star$  and surface filling factor  $f_s$  (assuming this filling factor does not vary significantly with height) is

$$l_{\max} = 2f_s \sqrt{h^2 + 2hR_\star}. \quad (6)$$

Considering typical parameters found for stellar coronae, we can estimate from the above equation whether or not we expect significant photon scattering in stellar coronae, regardless of whether we see a net photon loss. From Eq. 3 we can estimate the optical depth at the limb for Ne and O Ly $\alpha$  lines. Assuming the temperature of maximum formation of the line, i.e. about 6 MK and 3 MK for Ne and O respectively, and typical density of about  $10^{10} \text{ cm}^{-3}$  and

$10^{11} \text{ cm}^{-3}$  respectively (see e.g., TDP04, Ness et al. 2004), we derive  $\tau(\text{Ne}) \sim 5.2 \times 10^{-10} \cdot l_{\text{max}}$  and  $\tau(\text{O}) \sim 3.6 \times 10^{-10} \cdot l_{\text{max}}$ .

The height derived for coronal structures with different techniques (see §1 for references) is  $\lesssim R_{\star}/2$ ; on the Sun a typical coronal height is closer to  $R_{\star}/10$ . Assuming  $h = R_{\star}/10$ , and  $R_{\star} = R_{\odot}$  we obtain  $l_{\text{max}} \sim f_s \cdot 0.9R_{\star} \sim f_s \cdot 6 \times 10^{10} \text{ cm}$ .

Under these assumptions, the values of the optical depth at the limb, for a spherically symmetric corona, are therefore  $\tau(\text{Ne}) \sim 30f_s$  and  $\tau(\text{O}) \sim 20f_s$  (or  $\tau(\text{Ne}) \sim 80f_s$  and  $\tau(\text{O}) \sim 55f_s$  if we assume  $h = R_{\star}/2$ , and  $R_{\star} = R_{\odot}$ ). For the typical filling factors lower than a few percent (e.g., TDP04) we obtain optical depth  $\tau \lesssim 1$  both for Ne and for O.

### 6.3. Correlation of scattering with stellar and coronal parameters

While only three of our stellar sample present a significant case for resonance scattering, it is possible that trends of the departure from the theoretical  $\text{Ly}\alpha/\text{Ly}\beta$  ratio with fundamental stellar parameters can be found. We have examined the departures of observed from theoretical  $\text{Ly}\alpha/\text{Ly}\beta$  ratios as a function of X-ray surface flux, surface flux in the  $\text{Ly}\alpha$  line,  $L_X/L_{\text{bol}}$ , filling factors, and plasma density. These comparisons are suggestive of correlations between quenching of  $\text{Ly}\alpha$  photons and both  $L_X/L_{\text{bol}}$  and the density-sensitive ratio of strengths of the forbidden and intercombination lines,  $f/i$ , of Mg XI.

These correlations are illustrated in Figure 10 where we show the measured to theoretical ratios of O VIII  $\text{Ly}\alpha/\text{Ly}\beta$  of our sample as a function of  $L_X/L_{\text{bol}}$  (*top*) and Mg XI  $f/i$  (*bottom*). Error-weighted linear fits to the data in these figures yield slopes of  $-0.11 \pm 0.04$  and  $0.25 \pm 0.06$ , respectively. The sources presenting evidence of optical depth effects are the stars characterised by the highest activity level ( $L_X/L_{\text{bol}}$ ) and the highest plasma densities (i.e. lowest  $f/i$ ) in our sample. Such correlations are what are expected based on Eqn. 3. Optical depth is proportional to the product of electron density and typical path length within an emitting region,  $n_e \ell$ . For a given fixed volume emission measure,  $n_e^2 V \sim n_e^2 \ell^3$ , the optical depth varies as  $n_e^{1/3}$  or  $\ell^{-1/2}$ , and so increases with increasing plasma density. In the case of  $L_X/L_{\text{bol}}$ , an increase in  $L_X$  can arise through either  $\ell$  or  $n_e$ , such that any increase in  $L_X$  might typically be expected to lead to greater scattering optical depth. While only a small handful of our measurements present truly significant detections of resonance scattering, the evidence for trends of increasing  $\tau$  with  $L_X/L_{\text{bol}}$  and Mg XI  $f/i$  as is expected adds confidence to the interpretation of the  $\text{Ly}\alpha/\text{Ly}\beta$  ratios in these terms.

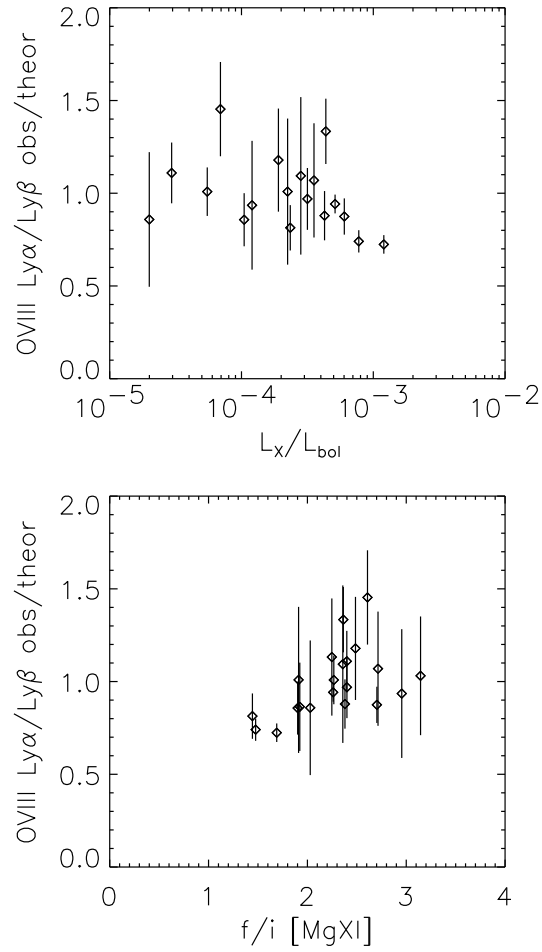


Fig. 10.— Ratios of measured to theoretical O VIII Ly $\alpha$ /Ly $\beta$  ratios plotted vs.  $L_X/L_{\text{bol}}$  (*top*) and vs. the Mg XI forbidden to intercombination line ratio (from TDP04; *bottom*), which is a diagnostic of plasma density (low  $f/i$  ratios correspond to high density).

## 7. Conclusions

We have investigated the optical thickness of stellar coronae through the analysis of  $\text{Ly}\alpha$  and  $\text{Ly}\beta$  lines of hydrogen-like oxygen and neon ions, in *Chandra*-HETG spectra of a large sample of active stars. Our study indicates that most stellar coronae are characterised by negligible visible signs of optical depth, in agreement with the results of previous studies based on Fe XVII lines. This indicates that coronae are either in general optically-thin, or that for cases in which optical depths reach of order unity or higher the geometry does not strongly favour lines-of-sight showing net  $\text{Ly}\alpha$  photon loss.

We do find evidence of significant optical depth in the O VIII Lyman lines of the RS CVn binary II Peg, and of the single M dwarf EV Lac; the RS CVn binary IM Peg also shows depletion of both Ne and O  $\text{Ly}\alpha/\text{Ly}\beta$  ratios as compared with theoretical predictions, and our analysis indicates that it is a transient effect present only in part of the observations. The detection of significant optical depth allows to derive an estimate for the photon path length and therefore for the typical height of the corona. The size of coronal structures derived for all three sources is of the order of a few percent of the stellar radius at most, implying very small coronal filling factors and high surface heating fluxes. We searched for correlation with basic stellar parameters and coronal properties and we find that the sources presenting evidence of significant optical depth are at the high end of activity level, with  $L_X/L_{\text{bol}}$  at the saturation limit, and high densities in their hot plasma, as revealed by the Mg XI He-like triplet lines.

For the stellar sample as a whole, we also find evidence of increasing quenching of  $\text{Ly}\alpha$  relative to  $\text{Ly}\beta$  as function of both  $L_X/L_{\text{bol}}$  and the density-sensitive Mg XI forbidden to intercombination line ratio. Such a trend is expected in the scenario in which optical depths are significant but generally small: viewing geometry rarely favours large net photon enhancements, but for favourable lines-of-sight photon depletion is expected to increase with both increasing  $L_X$  and increasing plasma density.

PT and DH were supported by SAO contract SV3-73016 to MIT for support of the *Chandra X-ray Center*, which is operated by SAO for and on behalf of NASA under contract NAS8-03060. JJD was supported by NASA contract NAS8-39073 to the *Chandra X-ray Center* during the course of this research. GP acknowledges support from Agenzia Spaziale Italiana and Italian Ministero dell'Università e della Ricerca.

## REFERENCES

- Audard, M., Güdel, M., Sres, A., Raassen, A. J. J., & Mewe, R. 2003, *A&A*, 398, 1137
- Audard, M., Telleschi, A., Güdel, M., Skinner, S. L., Pallavicini, R., & Mitra-Kraev, U. 2004, *ApJ*, 617, 531
- Berdyugina, S. V., Berdyugin, A. V., Ilyin, I., & Tuominen, I. 1998, *A&A*, 340, 437
- . 2000, *A&A*, 360, 272
- Berdyugina, S. V., Ilyin, I., & Tuominen, I. 1999, *A&A*, 347, 932
- Brickhouse, N. S., & Dupree, A. K. 1998, *ApJ*, 502, 918
- Brickhouse, N. S., Dupree, A. K., & Young, P. R. 2001, *ApJ*, 562, L75
- Brickhouse, N. S., & Schmelz, J. T. 2006, *ApJ*, 636, L53
- Brinkman, A. C., Behar, E., Güdel, M., Audard, M., den Boggende, A. J. F., Branduardi-Raymont, G., Cottam, J., Erd, C., den Herder, J. W., Jansen, F., Kaastra, J. S., Kahn, S. M., Mewe, R., Paerels, F. B. S., Peterson, J. R., Rasmussen, A. P., Sakelliou, I., & de Vries, C. 2001, *A&A*, 365, L324
- Canizares, C. R., Davis, J. E., Dewey, D., Flanagan, K. A., Galton, E. B., Huenemoerder, D. P., Ishibashi, K., Markert, T. H., Marshall, H. L., McGuirk, M., Schattenburg, M. L., Schulz, N. S., Smith, H. I., & Wise, M. 2005, *PASP*, 117, 1144
- Canizares, C. R., Huenemoerder, D. P., Davis, D. S., Dewey, D., Flanagan, K. A., Houck, J., Markert, T. H., Marshall, H. L., Schattenburg, M. L., Schulz, N. S., Wise, M., Drake, J. J., & Brickhouse, N. S. 2000, *ApJ*, 539, L41
- Chen, G.-X., & Pradhan, A. K. 2005, *astro-ph/0510534*
- Chung, S. M., Drake, J. J., Kashyap, V. L., Lin, L., & Ratzlaff, P. W. 2004, *ApJ*, 606, 1184
- Doron, R., & Behar, E. 2002, *ApJ*, 574, 518
- Drake, J. J. 2003, *Advances in Space Research*, 32, 945
- Drake, J. J., Brickhouse, N. S., Kashyap, V., Laming, J. M., Huenemoerder, D. P., Smith, R., & Wargelin, B. J. 2001, *ApJ*, 548, L81
- Drake, J. J., Peres, G., Orlando, S., Laming, J. M., & Maggio, A. 2000, *ApJ*, 545, 1074

- Favata, F., Micela, G., Reale, F., Sciortino, S., & Schmitt, J. H. M. M. 2000a, *A&A*, 362, 628
- Favata, F., Reale, F., Micela, G., Sciortino, S., Maggio, A., & Matsumoto, H. 2000b, *A&A*, 353, 987
- García-Alvarez, D., Drake, J. J., Ball, B., Lin, L., & Kashyap, V. L. 2006, *ApJ*, 638, 1028
- Golub, L., Hartquist, T. W. & Quillen, A. C. 1989, *Sol. Phys.*, 122, 245
- Grevesse, N., & Sauval, A. J. 1998, *Space Science Reviews*, 85, 161
- Gu, M. F. 2003a, *ApJ*, 582, 1241
- . 2003b, *ApJ*, 593, 1249
- Hatzes, A. P., Vogt, S. S., Ramseyer, T. F., & Misch, A. 1996, *ApJ*, 469, 808
- Huenemoerder, D. P., Canizares, C. R., Drake, J. J., & Sanz-Forcada, J. 2003, *ApJ*, 595, 1131
- Huenemoerder, D. P., Canizares, C. R., & Schulz, N. S. 2001, *ApJ*, 559, 1135
- Huenemoerder, D. P., Testa, P., & Buzasi, D. L. 2006, *ApJ*, 650, 1119
- Hussain, G. A. J., van Ballegooijen, A. A., Jardine, M., & Collier Cameron, A. 2002, *ApJ*, 575, 1078
- Kaastra, J. S., & Mewe, R. 1995, *A&A*, 302, L13+
- Kashyap, V., & Drake, J. J. 2000, *Bulletin of the Astronomical Society of India*, 28, 475
- Kastner, J. H., Huenemoerder, D. P., Schulz, N. S., Canizares, C. R., & Weintraub, D. A. 2002, *ApJ*, 567, 434
- Kastner, S. O., & Kastner, R. E. 1990, *Journal of Quantitative Spectroscopy and Radiative Transfer*, 44, 275
- Kerr, F. M., Rose, S. J., Wark, J. S., & Keenan, F. P. 2004, *ApJ*, 613, L181
- Landi, E., Del Zanna, G., Young, P. R., Dere, K. P., Mason, H. E., & Landini, M. 2006, *ApJS*, 162, 261
- Landi, E., & Gu, M. F. 2006, *ApJ*, 640, 1171

- Maggio, A., Pallavicini, R., Reale, F., & Tagliaferri, G. 2000, *A&A*, 356, 627
- Marino, A., Micela, G., Peres, G., & Sciortino, S. 2003, *A&A*, 407, L63
- Matranga, M., Mathioudakis, M., Kay, H. R. M., & Keenan, F. P. 2005, *ApJ*, 621, L125
- Mazzotta, P., Mazzitelli, G., Colafrancesco, S., & Vittorio, N. 1998, *A&AS*, 133, 403
- Mewe, R., Kaastra, J. S., van den Oord, G. H. J., Vink, J., & Tawara, Y. 1997, *A&A*, 320, 147
- Mitra-Kraev, U. 2006, Proceedings of “High Resolution X-ray Spectroscopy: towards XEUS and Con-X”, Ed. Branduardi-Raymont, G., p.E22
- Mitrou, C. K., Mathioudakis, M., Doyle, J. G., & Antonopoulou, E. 1997, *A&A*, 317, 776
- Morton, D. C. 2003, *ApJS*, 149, 205
- Ness, J.-U., Güdel, M., Schmitt, J. H. M. M., Audard, M., & Telleschi, A. 2004, *A&A*, 427, 667
- Ness, J.-U., & Schmitt, J. H. M. M. 2005, *A&A*, 444, L41
- Ness, J.-U., Schmitt, J. H. M. M., Audard, M., Güdel, M., & Mewe, R. 2003, *A&A*, 407, 347
- Phillips, K. J. H., Greer, C. J., Bhatia, A. K., Coffey, I. H., Barnsley, R., & Keenan, F. P. 1997, *A&A*, 324, 381
- Phillips, K. J. H., Greer, C. J., Bhatia, A. K., & Keenan, F. P. 1996, *ApJ*, 469, L57+
- Phillips, K. J. H., Mathioudakis, M., Huenemoerder, D. P., Williams, D. R., Phillips, M. E., & Keenan, F. P. 2001, *MNRAS*, 325, 1500
- Pradhan, A. K. 1985, *ApJ*, 288, 824
- Reale, F., Güdel, M., Peres, G., & Audard, M. 2004, *A&A*, 416, 733
- Redfield, S., Ayres, T. R., Linsky, J. L., Ake, T. B., Dupree, A. K., Robinson, R. D., & Young, P. R. 2003, *ApJ*, 585, 993
- Rosner, R., Tucker, W. H., & Vaiana, G. S. 1978, *ApJ*, 220, 643
- Saba, J. L. R., Schmelz, J. T., Bhatia, A. K., & Strong, K. T. 1999, *ApJ*, 510, 1064
- Sanz-Forcada, J., Brickhouse, N. S., & Dupree, A. K. 2002, *ApJ*, 570, 799

- . 2003a, *ApJS*, 145, 147
- Sanz-Forcada, J., Maggio, A., & Micela, G. 2003b, *A&A*, 408, 1087
- Scelsi, L., Maggio, A., Peres, G., & Gondoin, P. 2004, *A&A*, 413, 643
- Schmelz, J. T., Saba, J. L. R., Chauvin, J. C., & Strong, K. T. 1997, *ApJ*, 477, 509
- Schmitt, J. H. M. M., & Favata, F. 1999, *Nature*, 401, 44
- Schuessler, M., Caligari, P., Ferriz-Mas, A., Solanki, S. K., & Stix, M. 1996, *A&A*, 314, 503
- Smith, R. K., Brickhouse, N. S., Liedahl, D. A., & Raymond, J. C. 2001, *ApJ*, 556, L91
- Strassmeier, K. G., Hall, D. S., Fekel, F. C., & Scheck, M. 1993, *A&AS*, 100, 173
- Testa, P., Drake, J., & Peres, G. 2004a, *ApJ*, 617, 508
- Testa, P., Drake, J., Peres, G., & DeLuca, E. 2004b, *ApJ*, 609, L79
- Testa, P., Peres, G., & Reale, F. 2005, *ApJ*, 622, 695
- Testa, P., Reale, F., Garcia-Alvarez, D., & Huenemoerder, D. 2007, *ApJ*, in press
- Vaiana, G. S., Fabbiano, G., Giacconi, R., Golub, L., Gorenstein, P., Harnden, F. R., Cassinelli, J. P., Haisch, B. M., Johnson, H. M., Linsky, J. L., Maxson, C. W., Mewe, R., Rosner, R., Seward, F., Topka, K., & Zwaan, C. 1981, *ApJ*, 245, 163
- Vogt, S. S., Hatzes, A. P., Misch, A. A., & Kürster, M. 1999, *ApJS*, 121, 547
- Withbroe, G. L., & Noyes, R. W. 1977, *ARA&A*, 15, 363
- Wood, K., & Raymond, J. 2000, *ApJ*, 540, 563